

# Role of soft-iron impellers on the mode selection in the VKS dynamo experiment

André Giesecke,\* Frank Stefani, and Gunter Gerbeth

*Forschungszentrum Dresden Rossendorf*

(Dated: October 28, 2018)

A crucial point for the understanding of the von-Kármán-Sodium (VKS) dynamo experiment is the influence of soft-iron impellers. We present numerical simulations of a VKS-like dynamo with a localized permeability distribution that resembles the shape of the flow driving impellers. It is shown that the presence of soft-iron material essentially determines the dynamo process in the VKS experiment. An axisymmetric magnetic field mode can be explained by the combined action of the soft-iron disk and a rather small  $\alpha$ -effect parametrizing the induction effects of unresolved small scale flow fluctuations.

PACS numbers: 47.65.-d, 52.30.Cv, 52.65.Kj, 91.25.Cw

Keywords: dynamo,  $\alpha$ -effect, VKS experiment, permeability, kinematic induction equation, simulations

Homogenous dynamo action, i.e. the transformation of the kinetic energy of a flowing conducting fluid into magnetic energy, accounts for the generation of planetary, stellar and galactic magnetic fields. The last decade has seen tremendous progress in the experimental investigation of dynamo action [1]. By exploring parameter regions that are hardly accessible to numerical simulations, such experiments are essential for a better understanding of geo- and astrophysical magnetic fields. So far the threshold of magnetic field self-excitation has been crossed only in three liquid sodium experiments in Riga, Karlsruhe, and Cadarache. In the latter one, the von-Kármán-Sodium (VKS) experiment, a turbulent flow of liquid sodium is driven by two counter-rotating impellers located at the opposing end caps of a cylindrical domain, and field generation sets in when the magnetic Reynolds number exceeds the critical value of  $Rm^c \approx 32$  [2]. Besides of the rich dynamical behavior, including periodic and irregular field reversals that occur when the impellers rotate with different frequencies [3], the structure of the measured field attracts attention because of its high degree of axisymmetry [4]. This geometry is in contrast to all numerical predictions based on axisymmetric flows from which a magnetic field with an azimuthal wavenumber  $m = 1$  ( $B \propto \cos \varphi$ ) was expected [5–7]. Furthermore, dynamo action is only obtained when the impellers are made of soft-iron with a relative permeability of the order of  $\mu_r \approx 100$ . So far, there is neither a satisfying explanation of the observed axisymmetric field, nor of the failure of the dynamo in case that non-magnetic impellers are being used. This means, in turn, that the very working principle of the VKS dynamo is not understood at all. A first attempt to explain the axisymmetric mode in the VKS experiment was recently made in terms of a turbulent  $\alpha\omega$ -model [8, 9]. The consideration of turbulence seems imperative since the kinetic Reynolds number is of the order  $Re \sim 10^6$ , and flow and field exhibit strong fluctuations that are of the same order as the mean values. The model allows to circumvent the restrictions imposed by Cowling’s theorem which forbids

axisymmetric dynamo action [10]. Indeed, it was shown in [11] that an axisymmetric VKS-like flow supported by an  $\alpha$ -effect is able to excite an axisymmetric field. However, the magnitude of the  $\alpha$ -effect which is necessary to explain the dominant axial dipole turned out to be several times larger than the rms value of the turbulent velocity. Therefore, this simple  $\alpha\omega$ -model seems not capable of explaining the VKS dynamo mechanism. But what about the role of the soft-iron impellers? Originally, their use was motivated by the hope to shield off the field in the bulk of the cylinder from the lid layers behind the impellers. These layers, and particularly any rotating flow therein, had been shown to be extremely detrimental for dynamo action [7]. First attempts to investigate the role of the high permeability impellers utilized simplifying boundary conditions that enforce a vanishing tangential field at the top and the bottom of the cylindrical domain which mimics the field behaviour in case of end caps with infinite  $\mu_r$  [9, 12]. A similar approach was followed in [13] with focus on the impact of an additional non-axisymmetric velocity component with azimuthal wave number ( $m = 8$ ) that describes a hypothetical vortex structure between adjacent impeller blades. Comparable to the  $\alpha\omega$ -model with a localized  $\alpha$ -effect [9, 11], an axisymmetric field was obtained when the amplitude of the distortion is of the same order as the mean flow. This means, however, that a similar problem as for the  $\alpha\omega$ -model arises, because the assumed existence of highly correlated, large amplitude non-axisymmetric motions could not be confirmed in water experiments [14]. In this Letter, we will treat the rotating soft-iron impellers in a more realistic manner than just to assume vanishing tangential field conditions at the end caps. We consider dynamo action caused by an axisymmetric mean flow  $\mathbf{u}$  which might be supported by an  $\alpha$ -effect. The large scale magnetic flux density  $\mathbf{B}$  is governed by the mean field induction equation

$$\frac{\partial \mathbf{B}}{\partial t} = \nabla \times \left( \mathbf{u} \times \mathbf{B} + \alpha \mathbf{B} - \frac{1}{\mu_0 \sigma(\mathbf{r})} \nabla \times \frac{\mathbf{B}}{\mu_r(\mathbf{r})} \right). \quad (1)$$

Here  $\sigma$  denotes the conductivity,  $\mu_0$  the permeability of

vacuum and  $\mu_r$  the relative permeability. An  $\alpha$ -effect might be caused either by a gradient of the turbulence intensity or by helical fluid motions predominantly in-between the eight blades of the impeller disks. In the latter case, the ( $m = 8$ ) flow modulation is considered as a small scale variation whose averaged influence is parametrized by an axisymmetric  $\alpha$ -source term [9, 11]. From Eq. (1) it follows that a high (even if only localized) permeability  $\mu_r$  reduces the effective magnetic diffusivity  $\eta^{\text{eff}} = (\sigma\mu_0\mu_r^{\text{eff}})^{-1}$ , where  $\mu_r^{\text{eff}} = V^{-1} \int \mu_r(\mathbf{r})d^3r$  and  $V$  denotes the cylinder volume. In addition, the terms on the r.h.s. of Eq. (1) that involve gradients of  $\sigma$  or  $\mu_r$  are able to couple toroidal and poloidal field components in a way that possibly allows exponentially growing solutions for  $\mathbf{B}$ . A paradigm for this type of dynamo has been presented by Busse and Wicht [15] who showed that even a constant flow over an infinite plate with spatially varying conductivity is able to sustain a dynamo. Interestingly, the structure of the field is then determined by a constant part modulated by a contribution with the wave number of the conductivity variation. A similar effect results from the inhomogeneous permeability distribution in the VKS experiment, and it is worthwhile to check if this is already sufficient to explain a significant axisymmetric contribution. However, a purely axisymmetric field cannot be expected as such a solution is forbidden even in case of space- and time dependent permeability/conductivity distributions [16].

Eq. (1) is solved numerically applying a finite volume method [17]. Note that at the experimental temperature of  $\sim 120^\circ\text{C}$ , the differences of the electrical conductivity of iron and liquid sodium are not very important so that we focus on a non-uniform permeability distribution. In the grid based approach the implementation of spatially varying material coefficients is straightforward and only requires the application of a simple averaging directive for the reconstruction of the local (discretized) value of  $\mu_r$  that is seen by a field component at a certain grid cell. Although the scheme is easy to implement, the simulations are still demanding because large gradients of  $\mu_r$  must be resolved. To keep the computational time in a reasonable limit, the presented results are restricted to a maximum value of  $\mu_r = 60$ . This is in rough agreement with recent measurements of the permeability of a VKS-like impeller that gave values of  $\mu_r \approx 65 \dots 70$  [18].

A suitable mean flow that describes the velocity distribution in the VKS-experiment is represented by the so called MND-flow [19],

$$\begin{aligned} u_r(r, z) &= -\pi/H \cos(2\pi z/H) r(1-r)^2(1+2r), \\ u_\varphi(r, z) &= 4\epsilon r(1-r) \sin(\pi z/H), \\ u_z(r, z) &= (1-r)(1+r-5r^2) \sin(2\pi z/H), \end{aligned} \quad (2)$$

where  $H = 1.8$  denotes the distance between both impeller disks and  $\epsilon$  describes the relation between toroidal and poloidal component of the velocity. Here,  $\epsilon = 0.7259$

which is the optimum value for obtaining dynamo action, at least when the mean flow alone is considered. The entire model setup is visualized in the left panel of Fig. 1. The velocity field (2) is only applied in the region between the two impellers. The flow active region is restricted to a cylinder of radius  $R = 1$  (corresponding to 20.5 cm in the experiment) which is embedded in a layer of stagnant fluid with a thickness of  $0.4R$ . This so-called side layer significantly reduces  $\text{Rm}^c$  [7]. A lid layer is added behind

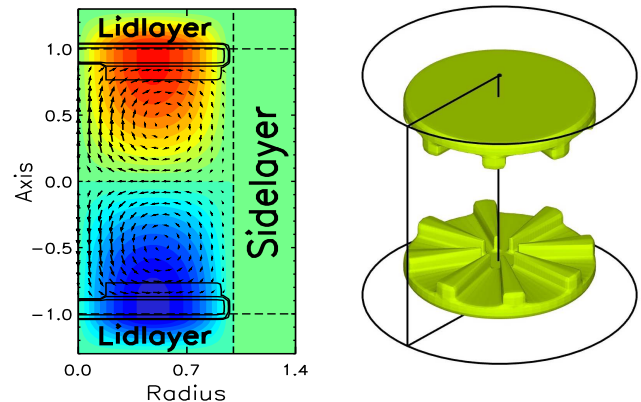


FIG. 1: Left panel: Structure of the prescribed axisymmetric velocity field. The color coded pattern represents the azimuthal velocity and the arrows show the poloidal velocity field. The black solid lines represent the shape of the impeller system (disk and blades). Right panel: assumed permeability distribution; isolevel at  $\mu_r = 35$  where the peak value is given by  $\mu_r = 40$ . In the fluid region  $\mu_r$  is equal to unity.

each impeller disk. Within these lid layers a purely rotating flow is assumed, modeled by a linear interpolation of the azimuthal velocity at the outer side of the impeller disk towards to zero at the end cap of the cylindrical domain. The presence of lid- and side layers reduces the influence of the magnetic boundary conditions so that, for the sake of simplicity, vanishing tangential field components are imposed at the outer surface of the computational domain. The solid black lines in the left panel of Fig. 1 represent isolevels of the permeability distribution that mimics the impellers with radius  $r = R$  and height  $h = 0.2$ . The impeller system is composed of two fractions: the disk, which is modeled by an axisymmetric scalar field with constant  $\mu_r \geq 1$ , and an azimuthally varying contribution located adjacent to the inner side of each disk. This part represents the system of eight blades and is modeled as an azimuthal rotating scalar field  $\propto \cos(8\varphi + \omega t)$  in a way that the minimum value (located between the blades) corresponds to  $\mu_r = 1$  (the permeability of the fluid) and the peak value corresponds to the disk permeability. Here,  $\omega$  denotes the angular velocity of the impeller that is necessary to drive a flow with a given  $\text{Rm}$  (defined as  $\text{Rm} = R\mu_0\sigma|U_{\text{max}}|$ ). The 3d structure of the resulting permeability distribution is shown in the right panel of Fig. 1. Note that the impellers are modeled only by the permeability distribution and no

particular flow boundary conditions are enforced on the (assumed) interface between impeller and fluid.

Initially, simulations have been performed without any  $\alpha$ -effect. After a transient phase that lasts approximately one diffusion time  $\tau \sim R^2/\eta^{\text{eff}}$ , the system settles in an eigenstate characterized by exponential growth, respectively decay,  $|\mathbf{B}| \sim e^{\gamma t}$  where  $\gamma$  denotes the field amplitude growth rate. Fig. 2 shows the growth rates for

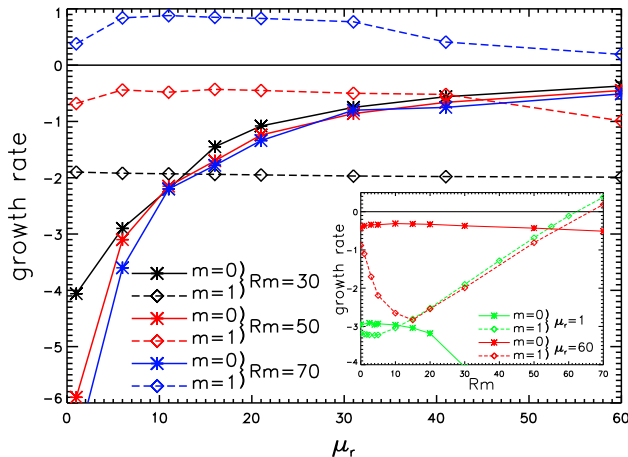


FIG. 2: Growth rates of the field amplitude (without  $\alpha$ -effect) Solid curves represent the results for the axisymmetric mode ( $m = 0$ ) and dashed curves show the ( $m = 1$ )-mode. The inset plot presents the growth rates for  $\mu_r = 1$  and  $\mu_r = 60$  in dependence on  $Rm$ .

the axisymmetric field mode ( $m = 0$ , solid curves) and the simplest non-axisymmetric mode  $B \propto \cos \varphi$  ( $m = 1$ , dashed curves). Even at moderate values of  $\mu_r$  the ( $m = 0$ )-growth rate is considerably shifted towards the dynamo threshold (but remains still negative). The reduction of this decay rate is roughly in agreement with the reduction of  $\eta_{\text{eff}}$ . For large permeabilities the growth rate of the axisymmetric mode saturates slightly below the dynamo threshold. In the experimental relevant interval ( $Rm \lesssim 50$ ) the ( $m = 0$ ) growth rate dominates and remains nearly independent of the applied  $Rm$ . Contrary to the axisymmetric mode, the ( $m = 1$ )-mode is hardly affected by the permeability distribution (for  $Rm \gtrsim 15$ ), and for sufficiently large  $Rm$ , the ( $m = 1$ )-mode dominates again, resulting in dynamo action around  $Rm^c \approx 60$ . Preliminary simulations applying only an axisymmetric distribution for the permeability (modeling the impeller disc without blades) exhibit a reduction of the ( $m = 1$ )-mode to  $Rm^c \approx 50$  whereas the axisymmetric field mode is hardly influenced (for  $Rm \lesssim 50$ ).

It is important to note that so far no growing axisymmetric solutions were obtained. One might have expected a sort of Busse-Wicht dynamo with an axisymmetric component modulated by a (unobserved) higher azimuthal wavenumber due to the azimuthally varying blade system. But evidently, this mechanism alone is

not sufficient to explain the occurrence of the dominant axisymmetric contribution in the VKS experiment. In the following we will see that an axisymmetric growing solution can be obtained if an additional small  $\alpha$ -effect is invoked. For the sake of simplicity we will assume

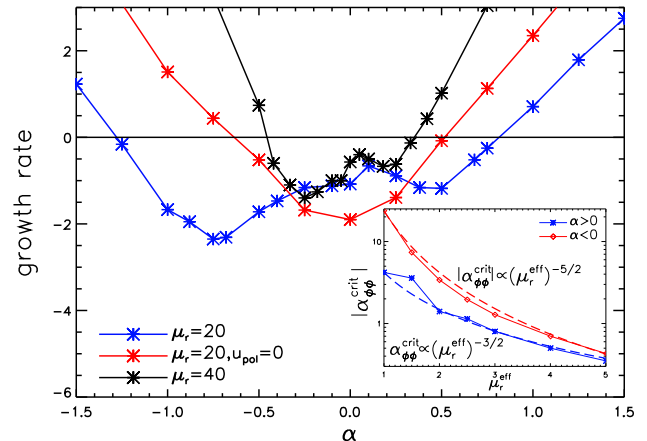


FIG. 3: Growth rates of the axisymmetric mode for  $Rm = 30$  in dependence of a prescribed homogenous  $\alpha$ -effect ( $\alpha_{\varphi\varphi}$ ). In all cases the ( $m=1$ )-mode lies below the growth rates of the axisymmetric solution. Additionally, the hypothetical case with  $\mathbf{u}_{\text{pol}} = u_r \mathbf{e}_r + u_z \mathbf{e}_z = \mathbf{0}$  has been studied for  $\mu_r = 20$ . The inset plot shows the scaling behavior of the critical value for  $\alpha_{\varphi\varphi}$  in dependence on  $\mu_r^{\text{eff}}$ .

a uniform distribution of  $\alpha_{\varphi\varphi}$ . This component is responsible for the generation of the poloidal field whereas the generation of the toroidal field essentially is determined by shear so that the other components,  $\alpha_{rr}$  and  $\alpha_{zz}$ , are assumed to be less important. Because the high permeability impellers have already shifted the growth rate of the ( $m = 0$ )-mode very close to zero, it is not surprising that a small  $\alpha$ -effect is now sufficient to excite a growing axisymmetric field even at moderate values of the impeller permeability (see Fig. 3). For larger  $\mu_r$  the dependence of the growth rates on the parameter  $\alpha$  is rather delicate and even a small variation in  $\alpha$  results in large changes of the corresponding growth rates. Growing axisymmetric fields are generated for both signs of  $\alpha$ , although they are obtained a bit more easily for positive values of  $\alpha$ . The critical value of  $\alpha_{\varphi\varphi}$  that is necessary for growing axisymmetric fields is strongly decreasing for increasing  $\mu_r$  (see inset plot in Fig. 3). In physical units the critical value for  $\mu_r = 40$  corresponds to  $|\alpha^c| \approx 0.15 \text{ ms}^{-1}$  which is much lower than the critical value reported in [11] where  $|\alpha^{\text{crit}}| \approx 16 \text{ ms}^{-1}$  was obtained (for  $\mu_r = 1$  and  $Rm = 32$ ). The local maxima for  $\mu_r = 20$  (blue curve) and  $\mu_r = 40$  (black curve) close to  $\alpha = 0$  correspond to stationary solutions whereas a transition to oscillating solutions occurs approaching the adjacent minima which might be the cause for the local suppression of the growth rate. Interestingly, the hypothetical omission

of the poloidal velocity component ( $\mathbf{u}_{\text{pol}} = u_r \mathbf{e}_r + u_z \mathbf{e}_z = \mathbf{0}$ ) works even in favor of the dynamo (see red curve in Fig. 3). This might explain the intriguing experimental observation that, despite a careful optimization of the impeller blades for one rotation direction, a change of this blade orientation does not alter significantly the critical Rm [4]. As long as the  $\alpha$ -effect close to the impellers is strong enough, poloidal field generation is sufficient to sustain the dynamo cycle. The resulting magnetic field is strongly concentrated in the impeller region (see Fig. 4a). For larger Rm, the field geometry is determined by the well known ( $m = 1$ ) dominated field structure (Fig. 4b) and dynamo action predominantly takes place in the bulk of the cylinder which explains the impassivity of the ( $m = 1$ )-mode towards the high  $\mu_r$  disks located close to the end caps. Note that in case

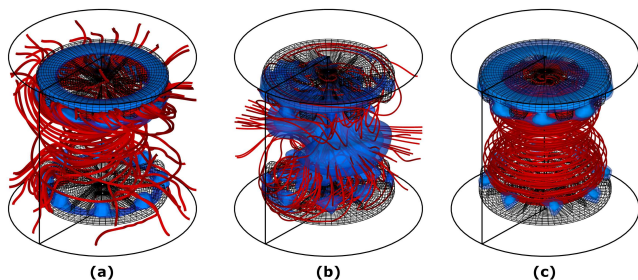


FIG. 4: Distribution of magnetic energy density (blue colored isosurfaces at 10% of the maximum value) and geometric structure of the magnetic field (red streamlines) for  $\mu_r = 20$ : (a)  $\text{Rm} = 30, \alpha = -1.5$ , growing axisymmetric mode; (b)  $\text{Rm} = 70, \alpha = 0$ , growing ( $m = 1$ )-mode; (c)  $\text{Rm} = 30, \alpha = 0$ , decaying axisymmetric mode. Note the ( $m = 8$ ) modulation induced by the impeller blades.

of a vanishing  $\alpha$ -effect the (decaying) solution is dominated by an axisymmetric toroidal field and the poloidal field generation is not sufficient to close the dynamo cycle (Fig. 4c). At this point, a deeper investigation requires a more detailed modeling of the  $\alpha$ -effect on the basis of water experiments. Direct numerical simulations of forced turbulence are far away from realistic parameters so that reliable models for the  $\alpha$ -distribution can hardly be extracted from DNS models. Preliminary simulations with a different spatial distribution of  $\alpha$  suggest that the extreme facilitation of the axisymmetric mode by the soft-iron disks is a generic effect which takes place as long as sufficient poloidal field generation (due to  $\alpha$ ) occurs nearby the impellers.

The dynamo process is strongly influenced by the reduction of  $\eta^{\text{eff}}$ . However, the decrease of  $\eta^{\text{eff}}$  is not sufficient to explain the results because simulations with the permeability variation replaced by a conductivity variation of the same magnitude (and space/time dependence) exhibit a significant deviation in the magnitude of the growth rates (although the tendency remains similar).

Our results clearly demonstrate that the common sim-

plified treatment of the high permeability impellers, by demanding vanishing tangential field components at the interface, is not justified. In the relevant range of Rm, the high permeability works selectively in favor of the ( $m = 0$ )-mode while the ( $m = 1$ )-mode is only slightly affected. To initiate a growing ( $m = 0$ )-mode, some  $\alpha$ -effect has still to be invoked, although the scaling behavior with  $\mu_r$  indicates that its magnitude is very small. The homogenous  $\alpha$ -distribution should be regarded as the simplest example how the soft iron disks facilitate growing axisymmetric solutions at reasonable parameter values. A complementary and more detailed approach will have to consider a non-axisymmetric flow variation in terms of azimuthally drifting equatorial vortices that have been observed in water experiments reported by [20]. Similar as in the  $\alpha$ -model with high permeability blades this should lead to a mixed mode solution of the magnetic field where a higher azimuthal mode is present.

We acknowledge fruitful discussions with A. Chiffaudel, F. Daviaud, S. Fauve, C. Gissinger, J. Léorat, C. Nore and J.-F. Pinton. Financial support from Deutsche Forschungsgemeinschaft in frame of the Collaborative Research Center SFB609 is gratefully acknowledged.

\* Electronic address: a.giesecke@fzd.de

- [1] F. Stefani, A. Gailitis, and G. Gerbeth, *Z. Angew. Math. Mech.* **88**, 930 (2008).
- [2] R. Monchaux *et al.*, *Phys. Rev. Lett.* **98**, 044502 (2007).
- [3] M. Berhanu *et al.*, *Europhys. Lett.* **77**, 59001 (2007).
- [4] R. Monchaux *et al.*, *Phys. Fluids* **21**, 035108 (2009).
- [5] L. Marié, J. Burguete, F. Daviaud, and J. Léorat, *Eur. J. Mech. B* **33**, 469 (2003).
- [6] F. Ravelet, A. Chiffaudel, F. Daviaud, and J. Léorat, *Phys. Fluids* **17**, 7104 (2005).
- [7] F. Stefani *et al.*, *Eur. J. Mech. B* **25**, 894 (2006).
- [8] F. Pétrélis, N. Mordant, and S. Fauve, *Geophys. Astrophys. Fluid Dyn.* **101**, 289 (2007).
- [9] R. Laguerre *et al.*, *Phys. Rev. Lett.* **101**, 104501 (2008), (see also erratum, **101**, 219902 (2008)).
- [10] T. G. Cowling, *Mon. Not. R. Astr. Soc.* **94**, 39 (1933).
- [11] A. Giesecke *et al.*, arXiv:0905.3957v1 [*Geophys. Astrophys. Fluid Dyn.* (2010, in press)].
- [12] C. Gissinger, A. Iskakov, S. Fauve, and E. Dormy, *Europhys. Lett.* **82**, 29001 (2008).
- [13] C. Gissinger, *Europhys. Lett.* **87**, 39002 (2009).
- [14] J. Burguete, priv. comm.
- [15] F. H. Busse and J. Wicht, *Geophys. Astrophys. Fluid Dyn.* **64**, 135 (1992).
- [16] R. Hide and T. N. Palmer, *Geophys. Astrophys. Fluid Dyn.* **19**, 301 (1982).
- [17] A. Giesecke, F. Stefani, and G. Gerbeth, *Magnetohydrodynamics* **44**, 237 (2008).
- [18] G. Verhille and J.-F. Pinton (2009), priv. comm.
- [19] L. Marié, C. Normand, and F. Daviaud, *Phys. Fluids* **18**, 017102 (2004).
- [20] A. de la Torre and J. Burguete, *Phys. Rev. Lett.* **99**, 054101 (2007).